

Mini-Reviews

Scattering Studies of Plant Cell Walls

A M Donald and O M Astley

Cavendish Laboratory, Madingley Road, Cambridge CB3 0HE, UK

Received 10th December 2001; accepted in revised form 14th March 2002.

Introduction

Cellulose - a polysaccharide - is the major component of plant cell walls, and is the commonest of all biopolymers. $\sim 10^{11}$ tonnes of cellulose are produced every year, and its uses are myriad. It is a linear polymer with a high level of internal hydrogen bonding (both interchain and intrachain). The interchain H bonding renders it insoluble in water and many common solvents, whereas the intrachain hydrogen bonding renders the molecule stiff; it is known to exist in extended microfibrils within the cell wall. This paper uses both small and wide angle x-ray scattering to examine the organisation of the cellulose within the cell wall and the response of the system to tensile deformation. In order to understand the cellulose itself, flax was chosen for study, because its secondary cell wall is thick and is fairly pure cellulose. However many plants contain substantial amounts of minority polysaccharides. To mimic such cell wall composites, the model system of acetobacter-produced cellulose fermented with appropriate minor polysaccharides has been chosen for study. Finally, to explore the supramolecular organisation within the cell wall, microfocus WAXS experiments on the algae *chara* - which has giant cells - were carried out.

A typical structure for a plant cell is shown in Figure 1. All cells have a primary wall, which is soft and flexible so that it can expand as the cell grows. After growth has stopped, many cells develop a secondary cell wall, which is much more rigid and provides structural support. In flax, this secondary cell wall is particularly thick, making up to 90% of the total cross section of the cell. It is about 70-75% cellulose, and the plant is therefore particularly suitable for studying the cellulose microfibrils. These microfibrils are always locally highly oriented. However, it is generally believed [1], that

through the thickness of the secondary cell wall the orientation rotates systematically, the alignment with each plane of microfibrils being rotated slightly with respect to its neighbours. This arrangement - equivalent to plywood but on a much smaller scale - is known as helicoidal (Figure 2).

The microfibrils are the smallest building block in the cell wall, but there is a whole hierarchy of structures present as shown in Figure 1. Any of these structures can be many microns across and up to mm in length: their cross sectional area increases in the order microfibril (also known in flax as an elementary fibre), technical fibre, bast fibre bundle, up to the whole stem.

Experimental

Materials

Flax (*linum usitatissimum*) came from both uninked flax stems and extracted fibres from Cebeco, The Netherlands, and were kindly provided by ATO-DLO, Wageningen. The fibres had been extracted by warm water retting, or by soaking in ethanol for 24 hours at room temperature, and then the technical fibres removed by laboratory scale hackling. To position the fibres in the x-ray beam, approximately five to ten technical fibres were aligned, lightly stressed at each end with a small bulldog clip and glued onto a cardboard mount with Araldite. The unstretched fibre length was 20-30 mm.

Acetobacter-produced cellulose and its composites were kindly supplied by Dr Elisabeth Chanliaud, Unilever Research, Colworth, and were made as described in [2-4]. The strain *Acetobacter aceti* subspecies *xylinum* was used and was grown on a culture medium of glucose and salts. The composites grown were sheets or discs of several cm² area, up to 5mm thick, and containing up to 99%

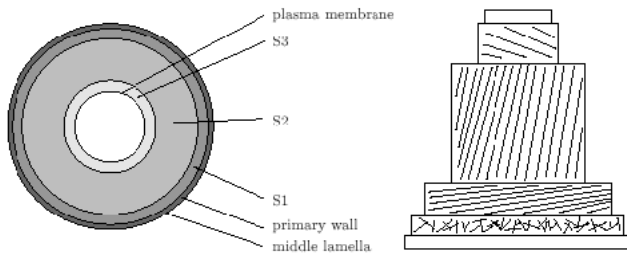


Figure 1: The traditional model of the plant cell wall of e.g wood cells, showing the different layers: S1, S2 and S3. The cellulose microfibrils are unaligned in the primary wall, and strongly aligned with different orientations in the S1, S2 and S3 wall layers.

water by weight. Composites were stored in 0.02% sodium azide solution in a refrigerator to prevent degradation. The composites used were incubated with either tamarind seed xyloglucan or apple pectin (DE 30 or 37).

Chara corallina var *australis* was kindly supplied by Professor Enid MacRobbie and grown by John Banfield at the Department of Plant Sciences, University of Cambridge. The plants had been grown in artificial pond water made up of 1mM NaCl, 0.4mM KCl and 0.1 mM CaSO₄. Cells were harvested from almost full grown plants, and pieces of the cell wall removed from both the internodal cells and the leaf cells. To remove the cell wall, the end of the cell was cut and the contents washed out with artificial pond water. The edge of the cylindrical cell was cut with a razor blade in the direction of the cell axis, and the cell was laid out flat onto a washer. Finally the cell wall was held in position by attaching pieces of mica over the ends of the cell wall and fixing these with Araldite.

Methods

Experiments were carried out on flax and acetobacter materials at the Daresbury synchrotron source, using stations 2.1, 8.2 and 16.1. A camera length of 3m was used for the acetobacter studies, and of 9m for the flax work. Data were collected with two dimensional gas-filled detectors. Where it was desirable to maintain the state of hydration, the flax fibres were wet before exposure by spraying with deionised water and using an environmental chamber. Tensile experiments were carried out either using a Minimat straining rig, or a purpose built tensometer in which both grips moved, permitting the region under study to remain centred

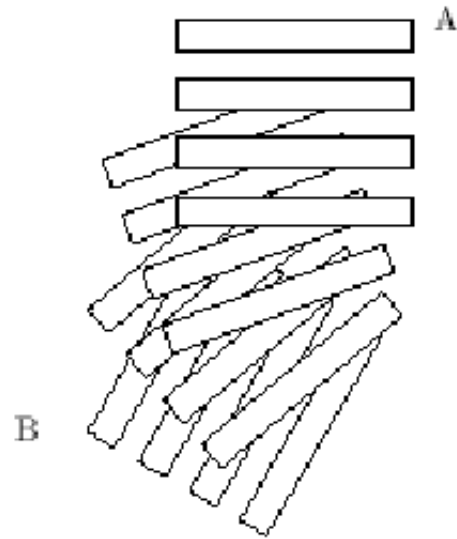


Figure 2 Surface view of a helicoid between layer A and layer B. The rectangles represent cellulose microfibrils and A and B might represent different layers in the cell wall. The angle between the layers in this case has been chosen to be 20°.

under the beam. Straining rates of 1mm/min were used for the acetobacter composites, and rates between 0.01 and 0.5 mm/min for the flax.

The experiments on *chara* were carried out at the ESRF, Grenoble on beamline ID13. A beam size of 2µm was used, with a wavelength of $\lambda=0.787\text{\AA}$. The scattering patterns were collected on a two-dimensional CCD camera in time steps of 30s to minimise beam damage. Using the movable sample stage with an optical microscope on ID13 allows positioning of the sample. For these cell wall samples, diffraction patterns were recorded either across the wall in a direction perpendicular to the cell axis, or around interesting features in the optical microscope in a grid. Step sizes of 10 and 20µm were used, with grid sizes of up to 200 x 200 µm².

Results and Discussion

Figure 3 shows a typical SAXS pattern from a horizontal bundle of flax fibres. A strong vertical (equatorial) streak is seen, which is broader in the wet sample (Figure 3b) than in the dry (Figure 3a). This streak arises from the microfibril scattering, and quantitative analysis of it can provide detail on the shape and dimensions of the microfibrils. From such figures, the one-dimensional small angle scattering intensity can be found by summing the intensity over a horizontal (or vertical) slice. $\hat{l}(q)$ is therefore equivalent to a slit-smear scattering pattern, although slit smearing does not occur for the

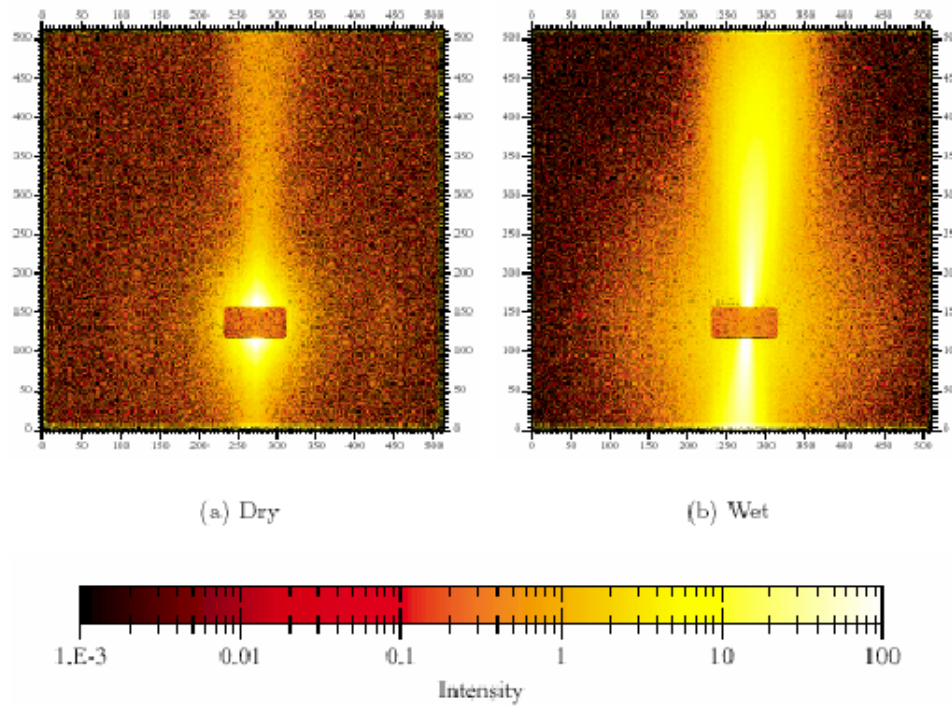


Figure 3 Typical SAXS patterns from flax fibres, recorded at $\lambda=1.4\text{\AA}$ with a camera length of approximately 3m, giving a q range of approximately $0.011\text{\AA}^{-1} < q < 0.20\text{\AA}^{-1}$. The fibre direction is horizontal. The two patterns are from the same sample, hydrated between exposures, of 2 min each.

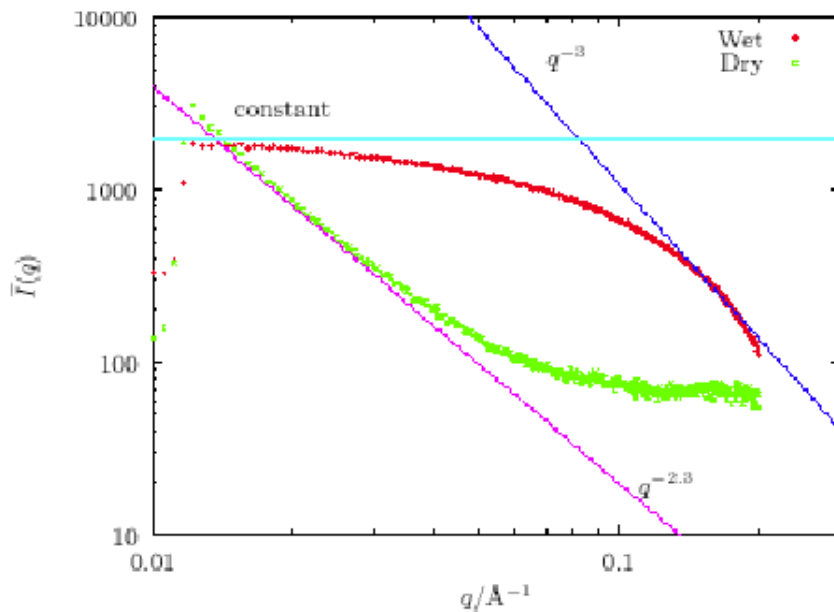


Figure 4 Plots of $\hat{I}(q)$ against q for very wet and very dry fibres, together with the $\hat{I}(q) = \text{constant}$ dependency predicted for long rods at low q , and the $\hat{I}(q) \propto q^{-3}$ dependency predicted by Porod's law at high q . The actual q dependency found at low q is also shown for the dry fibres.

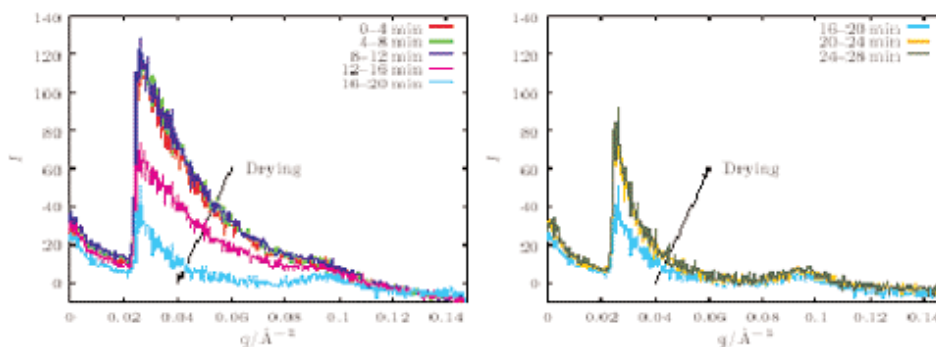


Figure 5 Meridional scattering patterns from drying flax fibres. The fibres were wet by spraying with deionised water and then letting them dry. The beam stop starts at $q = 0.24\text{\AA}^{-1}$, and the intensity below this value is due to a reduced direct beam.

Method	Minimum $r/\text{\AA}$	Maximum $r/\text{\AA}$
Guinier	18.7 ± 0.4	26.9 ± 0.3
Porod, $\phi = 0.47$	12.4 ± 0.2	15.6 ± 0.2
Via S	12.1 ± 0.1	19.3 ± 0.2
Via l_c	24.7 ± 0.1	28.3 ± 0.1

Table 1.

geometry of the Daresbury synchrotron (q is the scattering vector).

For a system of long rods, regardless of cross sectional shape, theory predicts that at low q , $\hat{I}(q) = \text{constant}$ [5]. At the other limit of large q , Porod's law states that $\hat{I}(q) \propto q^{-3}$. For the hydrated samples (Figure 4) shows that these expectations are borne out; however this is not the case for the dry fibres, where the shape of the $\hat{I}(q)$ vs q curve is very different. This is thought to be due to the microfibrils not scattering independently as assumed in arriving at these limiting laws (this has been shown to occur in other systems [6]): once the water is removed the microfibrils are no longer separated by water molecules. This leads to changes in the diffraction interference due to the concomitant changes in local scattering density.

If one starts off by making the further assumption that the rods are circular in cross section, with a radius of gyration r_c , and a cross sectional area S , then theory predicts the form of the scattering in the

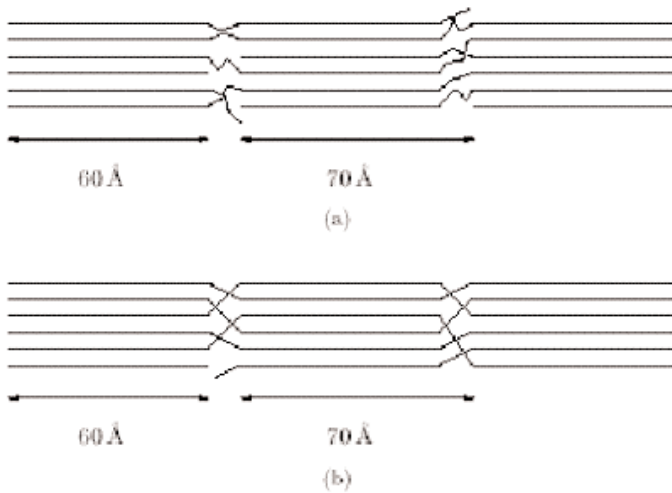


Figure 6 The postulated periodicity along the flax fibre axis, consisting of a crystalline region 6nm long followed by ~1nm of non-crystalline material. In a) the long period would be expected to increase on stretching since the molecules in the non-crystalline regions are not taut, but in b) this would not be expected. The lack of change in the long period upon stretching suggests b) is correct for flax.

two limits of small and large q . The Guinier approximation leads to

$$\hat{I}(q) = \text{const} \exp(-q^2 r_c^2 / 2) \quad [1]$$

and the Porod approximation at high q yields

$$\hat{I}(q) = \lim_{q \rightarrow \infty} \frac{1}{q^3} \frac{\hat{Q} C}{4S(1-\phi)} \quad [2]$$

where \hat{Q} is the invariant, C the circumference and ϕ the volume fraction of scattering elements. The invariant is defined by

$$\hat{Q} = \int_0^\infty q \hat{I}(q) dq \quad [3]$$

Alternative ways of calculating the dimensions of the fibrils also exist [7] using the invariant

$$S = \lim_{q \rightarrow \infty} \frac{2\pi \hat{I}(q)}{\hat{Q}} \quad [4]$$

and

$$l_c = \frac{2}{\hat{Q}} \int_0^\infty \hat{I}(q) dq \quad [5]$$

where l_c is the average chord length.

Table 1 shows the values of the radius obtained by these four different methods, with the spread of values obtained within a single method arising from data obtained on different samples. In order to use the Porod analysis to extract r , it is necessary to

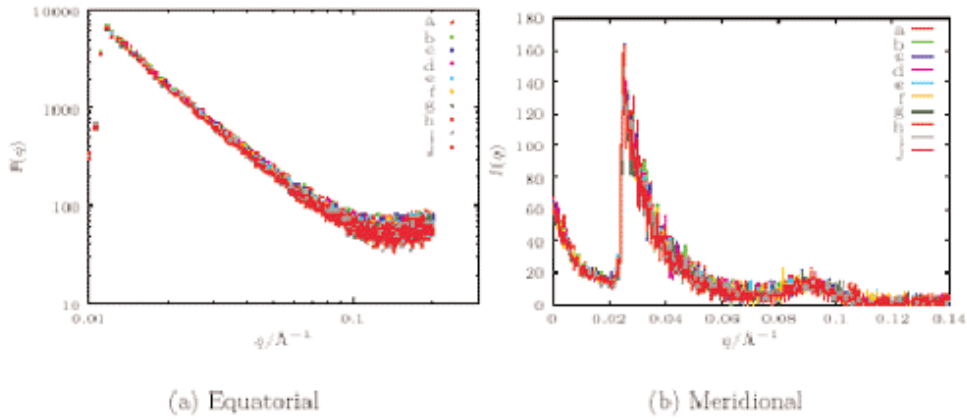


Figure 7 Plots of the equatorial and meridional intensities against q show no change in the scattering curves during stretching. Sample was dry flax stretched at 0.05mm/min. Curves $a-j$ correspond to data taken at intervals of extension of 0.1mm, with a corresponding to 0.05mm and j to 0.95mm extension.

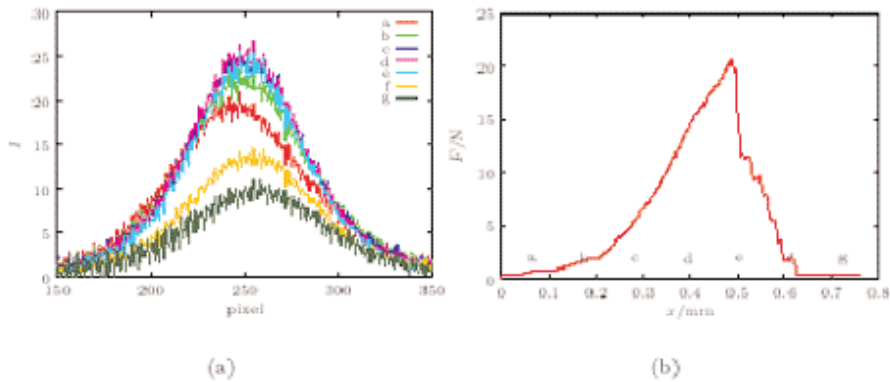


Figure 8 Changes in the (002) meridional peak of flax cellulose crystals as dry flax is stretched at 0.011mm/min. a) the orientation distribution, found by recording the variation in intensity along a line perpendicular to the meridian, at the position along the meridian of maximum breadth of the reflection across the wide angle detector; the letters indicate the position on the load-extension curve shown in b). As the WAXS detector in this set-up (simultaneous SAXS/WAXS) is off axis, the geometry is not precise.

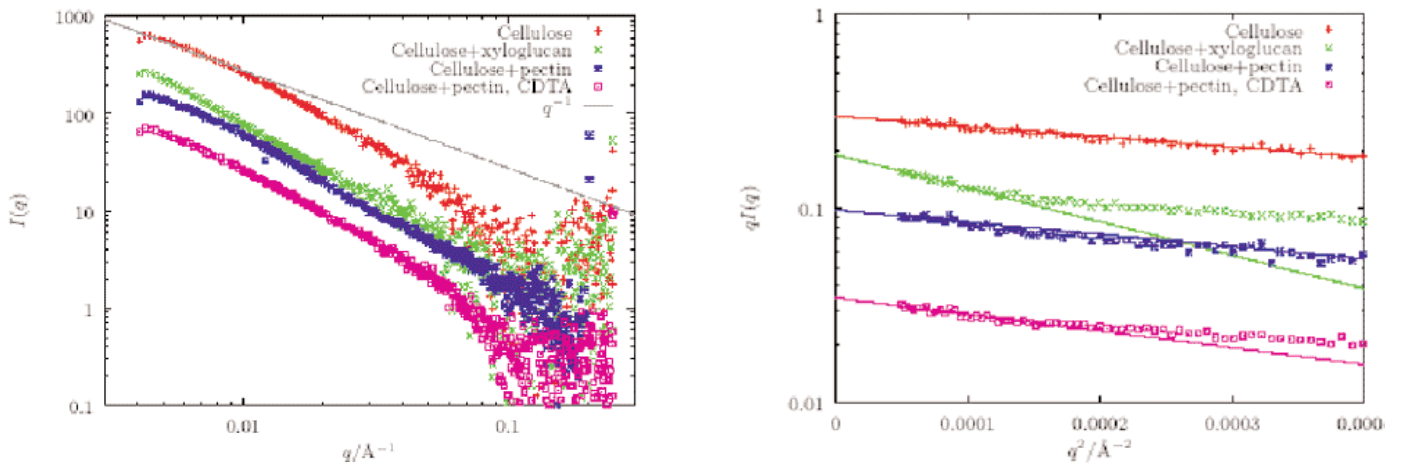


Figure 9:

a) Scattering curves from *acetobacter* composites. The data were collected from both 3m and 9m camera lengths and normalised to allow for different beam intensities. Data have been offset for clarity. Also shown is the scattering function $I(q) \propto q^{-1}$, which is predicted for long rods.

b) Guinier plot of $qI(q)$ against q^2 for low q for different *acetobacter* composites. Points are experimental data lines are Guinier fits over the range $0.007 < q < 0.01 \text{ \AA}^{-1}$, with a slope of $r_c^2/2$. The data have been offset for clarity.

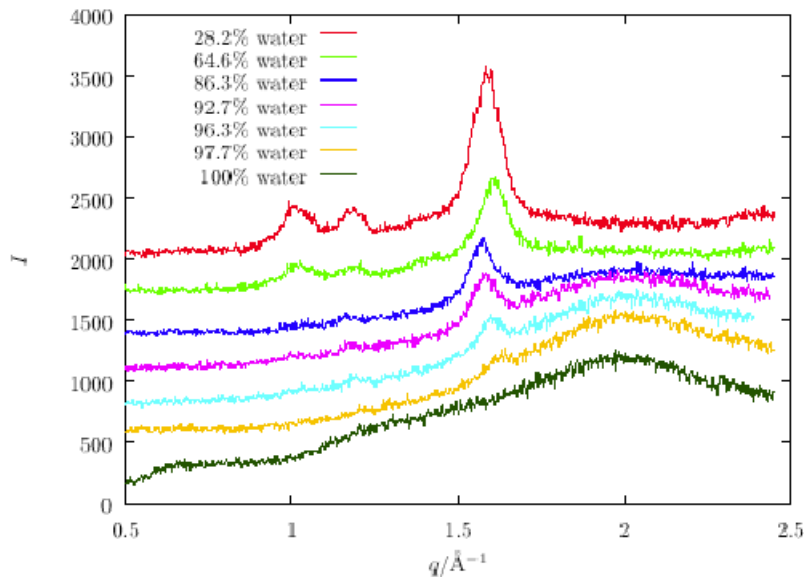


Figure 10 Powder X-ray diffractograms of *acetobacter* cellulose at different levels of hydration. Samples were dried by filter paper and by freeze drying; percentage of water is shown. Curves are offset for clarity. The pure water curve was obtained by holding between 2 sheets of mica.

assume both that the fibrils are cylindrical (i.e. have circular cross section) and a value for ϕ . This has been taken to be 0.47, an upper estimate based on the relative densities of the flax and crystalline cellulose [8]. As can be seen from the table, agreement between the different approaches is not good. This suggests that the original assumption of a circular cross section is not likely to be correct. A similar analysis can be carried out on the assumption the fibrils are rectangular. Based on this cross section values of $\sim 50 \times 10 \text{ \AA}$ are obtained, which is consistent with TEM evidence [9], but not with other SAXS data [10]. Thus the precise shape remains unclear. This section highlights the problem of trying to use SAXS to extract quantitative information on fibril shape and dimensions. Each method of analysis uses different approximations which affect the absolute numbers obtained. However TEM, although providing a more direct visualisation, introduces other problems such as potential artefacts during specimen preparation including the necessary dehydration and subsequent embedding in resin to permit cutting of ultrathin sections, and so is also not able to provide a reliable estimate of size.

So far we have only looked at the equatorial scattering. If we look at the meridional we find changes occurring during drying, as seen in Figure 5. In the scattering for the wet sample a faint shoulder is visible at $q \sim 0.1 \text{ \AA}^{-1}$, which becomes more pronounced upon drying. This position suggests a periodicity of 6-7 nm, presumably arising from alternating crystalline and amorphous regions along the chain direction. How this might arise is shown in

Figure 6. This model is discussed more fully in [11]. This meridional peak does not appear to have been observed in previous studies of cellulose I fibres, presumably because it is obscured by water scattering if the fibres are wet. Figure 5 demonstrates very clearly how the peak becomes more apparent as drying out occurs. It should be noted that hydrolysis studies of cellulose I have suggested much larger lengths for the crystallites in native cellulose. It therefore seems possible that two different crystal populations are coexisting in the fibre. The small crystals showing up here have a small dimension along the fibre, and a well-defined crystalline/non-crystalline repeat, unlike the larger crystals ($\sim 10 \text{ nm}$) previously reported [12]. Clearly the larger crystals dominate the scattering in general, and the 6nm crystals are only seen in rather dry fibres. Further discussion of this point is given in [11].

Let us now look at what happens when a tensile stress is applied to the flax fibre bundle. Figure 7 shows the results from the SAXS patterns. From this figure it is seen that no changes occur. Thus realignment of the microfibrils does not occur - they

Sample	$r_c/\text{\AA}$
Cellulose only	49 ± 9
Cellulose and xyloglucan	89 ± 4
Cellulose and pectin	54 ± 9
Cellulose and pectin, CDTA treated	63 ± 7

Table 2.

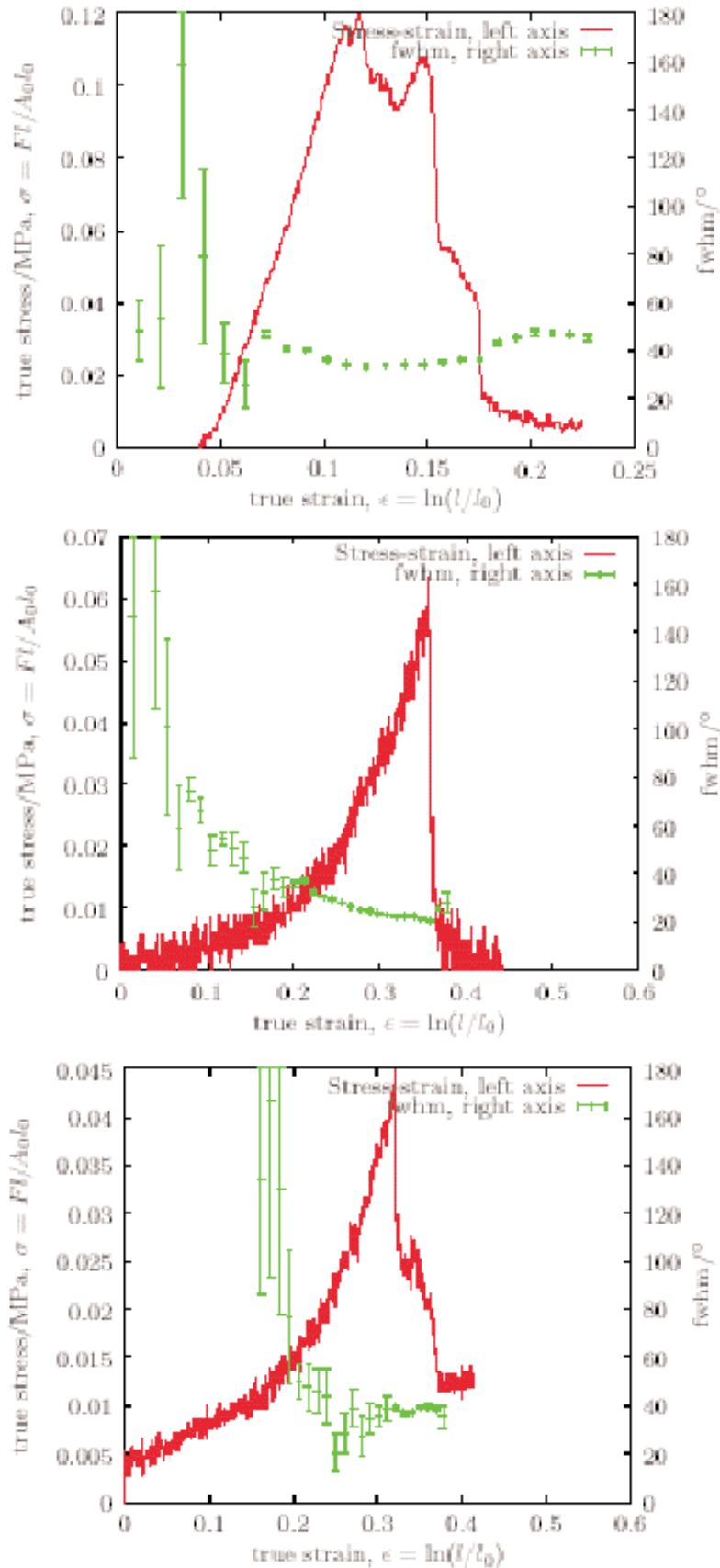


Figure 11 True stress-strain and misorientation (fwhm) curves for different *acetobacter* composites.

are already very well aligned - and the absence of changes in the meridional repeat means that this spacing is constant with stress. However changes are seen in the wide angle regime (Figure 8). Initially the intensity increases as the load increases up to the point where fracture occurs. Thereafter the intensity falls off, presumably due to some of the sample

having fallen out of the beam. Now since the SAXS signal has not changed, the overall repeat must be unchanged. Hence the increase in WAXS intensity seems likely to be related to strain induced crystallinity. Figure 8 shows how this can be achieved. The initial 6-7 nm repeat comprises a certain (unknown) percentage of amorphous

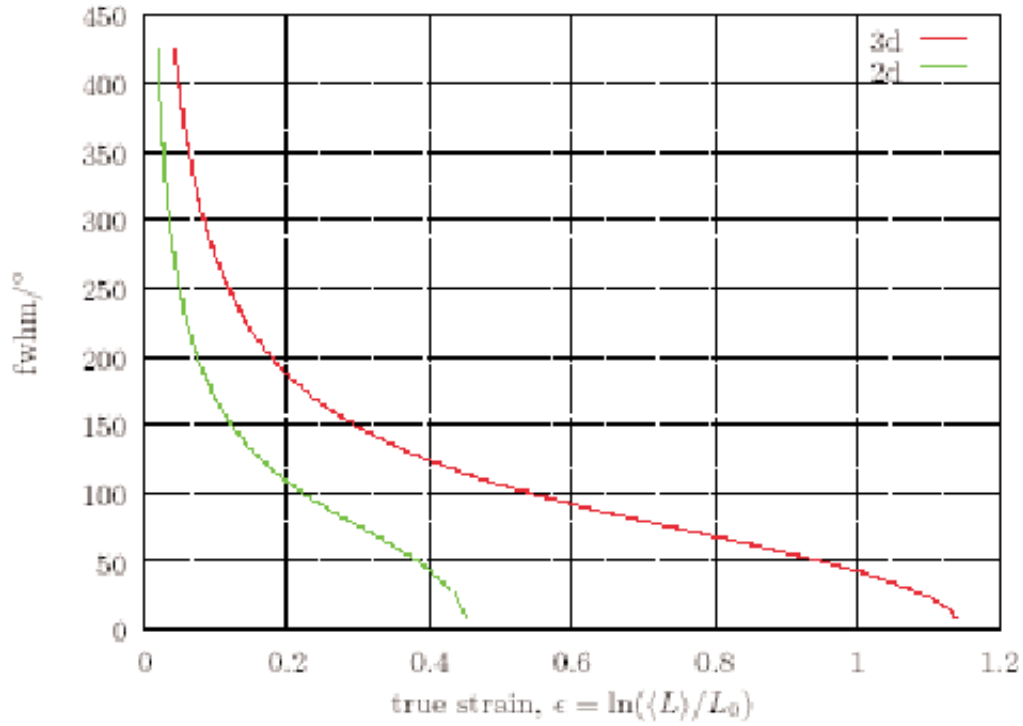


Figure 12 The expected strain produced by a Gaussian distribution of fibril orientations in two and three dimensions. Perfect orientation corresponds to $\langle L \rangle = 1$.

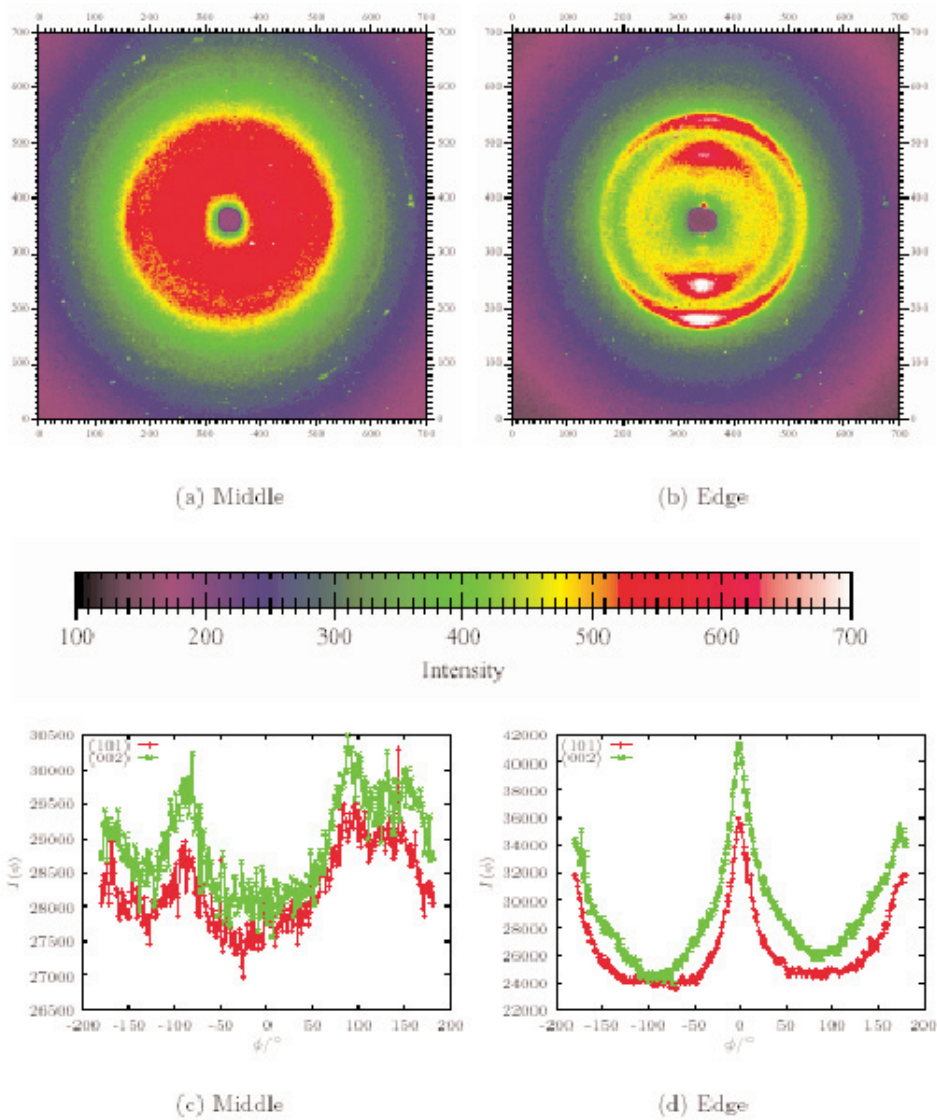


Figure 13 Scattering patterns taken from the middle and edge of a sample of a *chara* internodal cell wall. The two-dimensional images recorded on the detector are shown, together with the variation of the intensities for the (101) and (002) peak positions with angle. The meridional direction is horizontal.

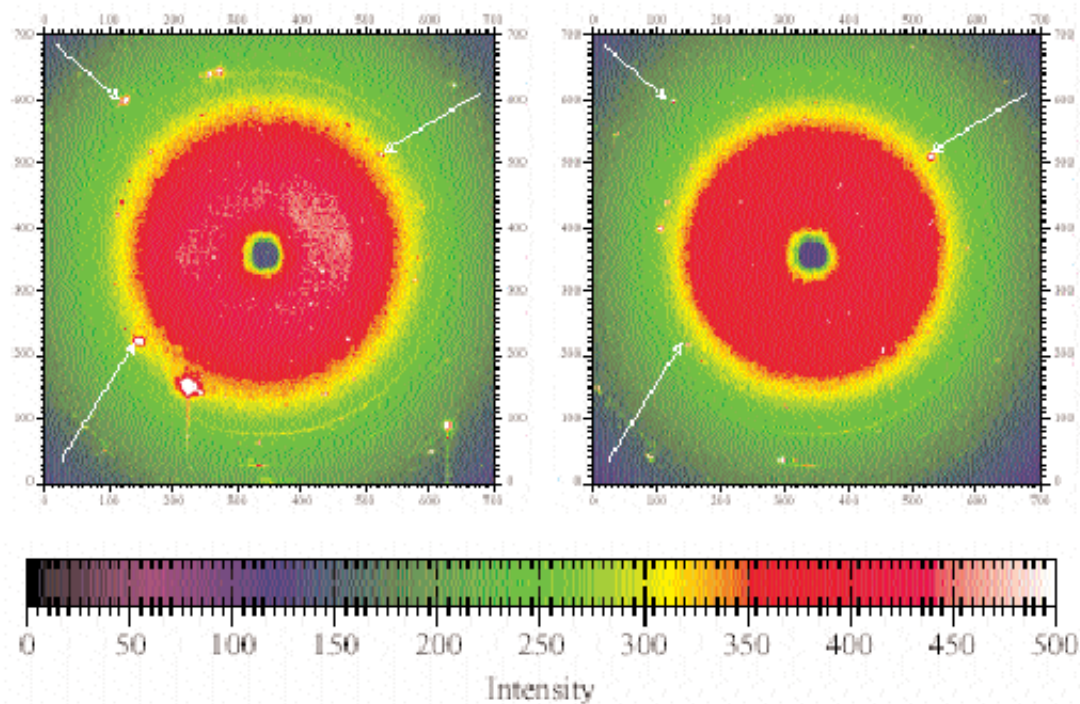


Figure 14 Diffraction patterns from the cell wall of a piece of *chara* leaf taken from adjacent 2 μm regions. Crystal peaks from the calcium carbonate in the same position in the two patterns are shown.

material. Under stress, some of this material can be pulled into better alignment and becomes incorporated into the crystals, thus increasing the overall level of crystallinity, without changing the overall repeat.

Acetobacter Results and Discussion

The bacterium *acetobacter xylinum* is known to produce cellulose in ribbon form usually in the cellulose I polymorph. By incubating the bacteria in a medium containing sugar and salt, pellicles of cellulose (incorporating water) can be produced. The inclusion of other polysaccharides in the incubation medium has been shown to lead to their incorporation in the pellicle [2].

SAXS of the different composites produced in this way are shown in Figures 9a. The Guinier approximation at low q was used to determine the radii of gyration for the microfibrils in each composite (Figure 9b) and the values obtained are shown in Table 2. It can be seen that the r_c determined is significantly larger for the xyloglucan composite than for the other systems. As in the work on flax, one presumes the fibrils are circular in cross section, which may not be a correct assumption. However, the differences between the different fibrillar building blocks for the different composites are small, and the difference in mechanical properties described below cannot be attributed to an

altered basic microstructure [13].

WAXS patterns on the as-produced pellicles showed no strong peaks, in contrast to previously obtained data (M Gidley, private communication). However these previous data had been obtained on freeze dried material. Figure 10 shows how the WAXS data (for pure cellulose) change as the water content is reduced, with the clear signature of cellulose I being visible below about 65 wt% water content (above this the peak is obscured). By using the Scherrer equation [14] on the (002) peak to estimate the size of the crystals

$$L_{002} = \frac{0.89\lambda}{\beta \cos \vartheta} \quad [6]$$

where λ is the wavelength of the radiation scattered through an angle 2θ , and β is the peak width in radians, it is found that the crystal size increases (non-linearly) with water content, with most of the increase occurring for water contents greater than 90%. The observed size for the (002) plane ranges from 5nm when dry to 10nm (assuming the crystals are perfect) when wet. This is in agreement with previous research on acetobacter cellulose [15]. Similar effects have also been seen on cotton [16], but in this case the crystal size increased at much lower water contents. It is suggested that the size increase arises from increased chain mobility in the

presence of water, permitting a higher percentage of the chains to move into the perfect register of the crystals. It cannot be due to recrystallisation, as this would occur in the more stable polymorph cellulose II.

The mechanical properties of the various composites are substantially different, as shown in Figure 11. The pure cellulose has a much higher breaking stress, and lower extensibility, than the composites. From the SAXS curves, it is possible to correlate the stress-strain curves with the reorientation revealed in the scattering patterns. Whereas for the fresh pellicle the scattering curves are isotropic, as loading proceeds the scattering starts to concentrate on the equator. The scattering intensity can be described by a Gaussian curve of the form

$$I(\phi) = A \exp\left(-\frac{(\phi - \langle \phi \rangle)^2}{2\sigma^2}\right) + \text{const} \quad (7)$$

where $\langle \phi \rangle$ is the mean fibril angle (normally essentially zero), σ is the standard deviation of the Gaussian and the constant is needed to take residual background scattering into account. Figure 11 shows the change in the full width half maximum of the $I(\phi)$ curves, equivalent to σ , for the different composites correlated with the stress strain curves. Despite the quantitatively very different stress-strain curves for the different samples, the shapes of the reorientation curves are very similar. Thus the rationale for the different mechanical properties cannot lie simply in the way the fibrils reorient.

However, if the system is modelled as a set of non-interacting rods it is possible to calculate the expected strain produced for different Gaussian distributions. To outline how this can be done, consider the simplest, if unrealistic, case of the fibrils (of length l) lying in a two-dimensional plane, with a distribution of fibril misorientations ϕ in the plane. The probability of the fibril lying at an angle between $\phi + d\phi$ is given by

$$P(\phi)d\Phi = \frac{(I(\phi) - c)}{\int_{-\pi/2}^{\pi/2} (I(\phi) - c)d\phi} d\phi \quad (8)$$

where c represents a constant to allow for residual background scattering. In this two dimensional case, the average length of a fibril in a direction parallel to

the tensile axis is given by

$$\langle L^{2d} \rangle = \int_{-\pi/2}^{\pi/2} lP(\phi) \cos \phi d\phi \quad (9)$$

The true strain of such an assembly of fibrils can therefore be calculated, and related to the standard deviation of the fibril misorientation σ . This permits the dependence of σ , and hence the fwhm of a peak in the scattering pattern, to be directly related to the strain (further details can be found in [17]). A similar calculation can be carried out in three dimensions. The form of such curves (Figure 12) is qualitatively different from those experimentally determined. It therefore appears that the microfibrils are not independent. Hence one possible explanation for the differences observed mechanically between the composites is that there are changes in the frequency of entanglement or crosslinking.

It is known that xyloglucan can form chemical crosslinks with cellulose [16] and the specific behaviour of any composite will depend on the comparative strengths of the cross links and entanglements which can form, with better alignment of the cellulose microfibrils tending to prevent entanglement. Thus it would seem that the detailed response of these composites is driven by the precise way in which entanglements or other constraints form between the cellulose and added biopolymer, and not differences in reorientation of the underlying fibrillar morphology.

Results and Discussion for Algae

Cells from the green algae *chara corallina* var. *Australis* were sliced open so that microfocus experiments could be carried out at different positions within the cell wall. Figure 13 shows WAXS patterns taken at the middle and edge of such a cell wall from regions 2 μ m across. These patterns confirm that cellulose I is present, as previously reported for the similar algae *nitella* [18]. Clear differences are seen in orientation between the two patterns, but these cannot be related to the occurrence of helicoids. Indeed, no signature of helicoids was seen in these microfocus experiments. In general the predominant orientation is perpendicular to the long axis of the cell. The strong orientation seen at the edge of the sliced-open cell wall is attributed to orientation induced by the cutting process.

The absence of any sign of helicoids does not in this case mean they are not present. It would appear that because the main microfibril orientation dominates the scattering pattern they cannot be resolved. This assumption is supported by plotting the expected azimuthal scans from a helicoid with different degrees of orientation (assumed to be Gaussian) and different angles between the layers. Such curves show that the ability to resolve the Gaussian peaks depends on both of these variables, and hence on the experimental signal to noise ratio. It is also interesting to note that striations are visible on the surface of the cell. These striations are attributed to alternating acid and base regions [19]. The absence of any systematic changes in the microfocus patterns possibly indicates that these striations are not related to simple orientational changes. Alternatively, as evidenced by the lack of observed helicoidal structures, the fact that one is examining a projection through the cell wall may wash out subtle variations in packing.

However what is observed to vary between different regions of the sample is the presence of sharp diffraction spots arising from crystals, which are clearly not due to cellulose. Figure 14 shows patterns obtained from two neighbouring regions (~20µm apart); some spots are seen to be common between these two patterns, but some spots also differ. Based on the total dataset obtained (50 different regions) it has proved possible to identify the crystals as calcium carbonate, and more specifically the calcite form. That calcium carbonate deposits exist on *chara* is well known - hence its common name of stonewort - but this study uniquely identifies the polymorph. Correlation of the crystal orientation with the underlying cellulose pattern also demonstrates that the presence of the calcite crystals does not affect the orientation of the microfibrils.

Conclusions

Using three rather different types of systems combined with both small and wide angle (including microfocus) scattering, it has been possible to probe different properties of the plant cell wall. The dimensions of the basic fibrillar building block can be established by fitting the SAXS curves. However, there is still some ambiguity about the precise dimensions, since the fit is model-dependent. It is also clear that there is some long-range periodicity, at the 6-7nm length scale, associated with regions of

good and poorer packing along the fibril direction. The meridional peak associated with this repeat in flax can only be seen in rather dry fibres.

Looking at cellulose composites provides an additional level of complexity, compared with the rather pure cellulose of flax. In this case it becomes clear that the differences in the fibrillar morphology between the different composites and in comparison with pure cellulose are small. Nevertheless the mechanical properties, as revealed by load extension curves collected simultaneously with SAXS/WAXS show substantial differences. These differences have been attributed to different degrees of connectivity between the fibrillar building blocks, associated with entanglements or crosslinking.

Finally, microfocus experiments have proved that the optical striations seen on the surface of the giant cells of the algae *chara* cannot be related to periodic variations in the underlying orientation of the cellulose fibrils. The only orientational differences observed appeared to be artefactual due to the cutting required during sample preparation. Using microfocus it has been possible to study the polymorphs of the small calcium carbonate crystals known to form on the surface of the plant. These have been shown to be of the calcite polymorph.

Acknowledgements

The authors are grateful to the BBSRC for funding. The assistance of all the beamline scientists is gratefully acknowledged (Anthony Gleeson, Günter Grossman, Sue Slawson, Nick Terrill, Martin Müller and Christian Riekel). The assistance of Drs Gidley, Chanliaud, John Banfield and Harriette Bos with sample supply is also acknowledged with thanks.

References

- [1] Neville, A.C., *Biology of Fibrous Composites: development beyond the cell membrane*. 1993, Cambridge: CUP.
- [2] Whitney, S.E.C., Brigham, J.E., Darke, A.H., Reid, J.S.G., and Gidley, M.J., *The Plant Journal*, (1995) **8** 491-504.
- [3] Whitney, S.E.C., Brigham, J.E., Darke, A.H., Reid, J.S.G., and Gidley, M.J., *Carbohydrate Research*, (1998) **307** 299-309.

- [4] Chanliaud, E. and Gidley, M., *The Plant Journal*, (1999) **20** 25 - 35.
- [5] Gawronski, M., Aguirre, G., Conrad, H., Springer, T., and Stahmann, K.-P., *Macromols*, (1996) **29** 1516-1520.
- [6] Heyn, A.N.J., *J Appl phys*, (1955) **26** 1113-20.
- [7] Glatter, O. and Kratky, O., *Small angle X-ray scattering*. 1982: Academic Press.
- [8] Astley, O.M., *Scattering studies of cell wall polymers*, . 2000, Cambridge University.
- [9] Näslund, P., Vyong, R., and Chanzy, H., *Textile Res J*, (1988) **58** 414-7.
- [10] Müller, M., Czihak, C., Vogl, G., Fratzl, P., Schober, H., and Riekkel, C., *Macromols*, (1998) **31** 3953-57.
- [11] Astley, O.M. and Donald, A.M., *Biomacromols*, (2001) **2** 672-80.
- [12] Scallan, A.M., *Textile Res J* (1971) **41**, 647-53.
- [13] Astley, O.M., Chanliaud, E., Donald, A.M., and Gidley, M.J., *Int J Biol Macromol*, (2001) **29** 193-202.
- [14] Randall, J.T., *The diffraction of X-rays and electrons by amorphous solids, liquids and gases*. 1934, London: Chapman and Hall.
- [15] Fink, H.-P., Purz, H.J., Bohn, A., and Kunze, J., *Macromol Symp*, (1997) **120** 207-17.
- [16] Nakamura, K., Hatekeyama, T., and Hatekeyama, H., *Text Res J*, (1983) **53** 682-8.
- [17] Astley, O.M., PhD Thesis, University of Cambridge 2000.
- [18] Probine, M.C. and Preston, R.D., *J Exp Bot*, (1961) **12** 261-82.
- [19] Lucas, W.J. and Smith, F.A., *J Exp Bot*, (1973) **24** 1-14.